

Local thermal conductivity of inhomogeneous nano-fluidic films: A density functional theory perspective

Zongli Sun(孙宗利), Yanshuang Kang(康艳霜), and Yanmei Kang(康艳梅)

Citation: Chin. Phys. B, 2024, 33 (**4**): 046503. DOI: 10.1088/1674-1056/ad18a9
Journal homepage: http://cpb.iphy.ac.cn; http://iopscience.iop.org/cpb

What follows is a list of articles you may be interested in

Transport properties of CrP

Xuebo Zhou(周学博), Ping Zheng(郑萍), Wei Wu(吴伟), Yu Sui(隋郁), and Jianlin Luo(雒建林)
Chin. Phys. B, 2023, 32 (**7**): 076501. DOI: 10.1088/1674-1056/acc80c

Molecular dynamics study on the dependence of thermal conductivity on size and strain in GaN nanofilms

Ying Tang(唐莹), Junkun Liu(刘俊坤), Zihao Yu(于子皓), Ligang Sun(孙李刚), and Linli Zhu(朱林利)
Chin. Phys. B, 2023, 32 (**6**): 066502. DOI: 10.1088/1674-1056/acbf26

Lattice thermal conductivity switching via structural phase transition in ferromagnetic VI_3

Chao Wu(吴超) and Chenhan Liu(刘晨晗)
Chin. Phys. B, 2023, 32 (**5**): 056502. DOI: 10.1088/1674-1056/acb764

Effects of phonon bandgap on phonon-phonon scattering in ultrahigh thermal conductivity ϑ-phase TaN

Chao Wu(吴超) and Chenhan Liu(刘晨晗)
Chin. Phys. B, 2023, 32 (**4**): 046502. DOI: 10.1088/1674-1056/acb201

Unusual thermodynamics of low-energy phonons in the Dirac semimetal Cd_3As_2

Zhen Wang(王振), Hengcan Zhao(赵恒灿), Meng Lyu(吕孟), Junsen Xiang(项俊森), Qingxin Dong(董庆新), Genfu Chen(陈根富), Shuai Zhang(张帅), and Peijie Sun(孙培杰)
Chin. Phys. B, 2022, 31 (**10**): 106501. DOI: 10.1088/1674-1056/ac8928

Local thermal conductivity of inhomogeneous nano-fluidic films: A density functional theory perspective

Zongli Sun(孙宗利)[1,3,†], Yanshuang Kang(康艳霜)[2], and Yanmei Kang(康艳梅)[4]

[1] *Department of Mathematics and Physics, North China Electric Power University, Baoding* 071003, *China*
[2] *College of Science, Hebei Agricultural University, Baoding* 071001, *China*
[3] *Hebei Key Laboratory of Physics and Energy Technology, Baoding* 071003, *China*
[4] *University of International Relations, Beijing* 100091, *China*

(Received 7 November 2023; revised manuscript received 8 December 2023; accepted manuscript online 26 December 2023)

Combining the mean field Pozhar–Gubbins (PG) theory and the weighted density approximation, a novel method for local thermal conductivity of inhomogeneous fluids is proposed. The correlation effect that is beyond the mean field treatment is taken into account by the simulation-based empirical correlations. The application of this method to confined argon in slit pore shows that its prediction agrees well with the simulation results, and that it performs better than the original PG theory as well as the local averaged density model (LADM). In its further application to the nano-fluidic films, the influences of fluid parameters and pore parameters on the thermal conductivity are calculated and investigated. It is found that both the local thermal conductivity and the overall thermal conductivity can be significantly modulated by these parameters. Specifically, in the supercritical states, the thermal conductivity of the confined fluid shows positive correlation to the bulk density as well as the temperature. However, when the bulk density is small, the thermal conductivity exhibits a decrease-increase transition as the temperature is increased. This is also the case in which the temperature is low. In fact, the decrease–increase transition in both the small-bulk-density and low-temperature cases arises from the capillary condensation in the pore. Furthermore, smaller pore width and/or stronger adsorption potential can raise the critical temperature for condensation, and then are beneficial to the enhancement of the thermal conductivity. These modulation behaviors of the local thermal conductivity lead immediately to the significant difference of the overall thermal conductivity in different phase regions.

Keywords: thermal conductivity, nano-fluidic films, density functional theory

PACS: 65.20.–w, 66.10.cd, 66.25.+g **DOI:** 10.1088/1674-1056/ad18a9

1. Introduction

Thermal conductivity is an essential parameter to characterize the thermal energy transfer in fluids. Accurate knowledge of thermal conductivity is conducive to understanding the underlying mechanisms in thermal-related processes.[1] As is known, it is also helpful to optimize and improve the efficiency of functional materials in their engineering applications.[2,3] In the past decades, a tremendous amount of effort has been devoted to the thermal conductivity of bulk fluids, and numerous approaches have been developed, including the empirical correlation method,[4] extended corresponding states model,[5] rough hard-sphere theory,[6] artificial neural network models,[7] and effective thermal conductivity models.[8,9] All these methods are efficient for prediction of thermal conductivity in bulk fluids, and have deepened our understanding about characteristics of thermal energy transfer in different application fields, e.g., thermal management of micro electronics,[10] energy conversion devices,[11] and energy storage systems.[12]

Rapid developments in nanoscience and nanotechnology have inspired increasing interests in fundamental investigations on thermal conductivity of confined fluids or nano-fluidic films.[13,14] One of the most significant features of thermal conductivity in such systems is its marked deviation from that of the corresponding bulk fluids. Although this creates unprecedented opportunities for the device development in the application domains, it also poses new challenges for modelling the thermal energy transfer on a nanoscale. On the theoretical aspect, molecular dynamics (MD) simulation has emerged as an efficient tool to study the thermal conductivity in confined fluids. Giannakopoulos *et al*. investigated the transport properties of liquid argon flowing in nanochannels by using of non-equilibrium MD simulation.[15] Their results suggest that the thermal conductivity increases with the increment of channel width. Applying the Green–Kubo approach in equilibrium MD simulations and the Müller–Plathe method in non-equilibrium MD simulations, Hyżorek and Tretiakov studied the thermal conductivity of liquid argon in nanochannels.[16] Both types of simulations reveal that the thermal conductivity depends weakly on the shape of channel and that it increases with the increment of the transversal size of the channel. Very recently, also by employing MD simulations, Jin *et al.* investigated the anisotropy of the thermal conductivity in liquid argon films.[17] Their results show that the

†Corresponding author. E-mail: sunzl@ncepu.edu.cn
© 2024 Chinese Physical Society and IOP Publishing Ltd

parallel thermal conductivity is enhanced by the solid–liquid interface, while the perpendicular thermal conductivity is reduced. In addition, the anisotropy of thermal conductivities is weakened with the increment of film thickness. It is worthy to emphasize that in all the above simulations, the thermal conductivity has been regarded as a whole, which serves only as an overall measurement of thermal energy transfer in confined fluids.

As for confined fluids, it is reasonable to suppose that the thermal transport should be position-dependent, due to its close correlation with the fluid structure. To our knowledge, only few investigations on the local thermal conductivity of confined fluids have been conducted, which is in sharp contrast to the situation for the overall thermal conductivity. Utilizing non-equilibrium MD simulations, Chilukoti *et al.*[18] studied the local thermal transport of liquid alkanes in the vicinity of α-quartz solid surfaces, and found that near the walls, the local thermal conductivity of the liquid alkane varies with position in an oscillating manner, which is similar to the local density profile. They also revealed that the thermal energy is less effectively transferred through the first adsorption layer near the wall than that in the central region. Recently, Zhao *et al.*[19] presented the molecular simulations on the thermal transport of water confined in nanochannels. They also found the inhomogeneous profiles of thermal conductivity, which is nearly in phase with the density profile. Actually, besides these MD simulations, some attempts have also been devoted by solving the classical kinetic equations. The most representative work is the one conducted by Pozhar and Gubbins (PG),[20,21] who solved the generalized Enskog-like kinetic equation with the aid of the 13-moments approximation, and derived the explicit, tractable expressions for the local transport coefficients for the inhomogeneous fluids. These obtained transport coefficients are particularly appealing, because they have been expressed in terms of equilibrium density and the contact value of radial distribution function. However, from the physical point of view, the PG derivation has placed itself on the level of mean field theory (MFT), which implies that the correlation effect could not be well considered, especially for the strongly inhomogeneous fluids. Therefore, some effective approaches for the correlation effect are still desiring.

In contrast to MFT, computer simulations can naturally consider the inter-particle correlation during the random sampling. Therefore, it is believed that the relevant results from simulations may shed beneficial lights on the correlation contribution of the thermal conductivity. In light of this, this work aims to propose a novel method for the local thermal conductivity of confined fluidic film by combining the PG result and some simulation-based correlations.[22,23] Within this method, the correlation beyond the mean field is considered through the weighted density calculation. It is necessary to emphasize that the only input in such a method is the equilibrium density of the fluidic film, which can be determined by utilizing of the classical density functional theory (DFT). This makes the proposal rather appealing and convenient in its application to the inhomogeneous fluids.

This work is organized as follows. In Section 2, the main results of the PG derivation are outlined. In Section 3, the method for the correlation contribution of the local thermal conductivity is proposed and analyzed. The DFT scheme is given in Section 4. In Sections 5 and 6, the proposed method is applied to the confined argon films in slit pores, and the influences of both the fluid parameters and the pore parameters on the thermal conductivity are investigated in detail. A short summary is finally given in Section 7.

2. PG theory for the local thermal conductivity

In the derivation of PG theory,[20] the inhomogeneous fluid is assumed to consist of nonreactive and structureless particles, which interact via a pair-additive, central potential, e.g., the Lennard–Jones (LJ) potential. Starting from the Liouville equation for the collective dynamic variables and introducing the generalized Mori projection operator technique, PG developed a functional perturbation theory for the evolution of the many-body dynamic system, which can be further simplified to the following kinetic equation:

$$\begin{aligned}&\left(\frac{\partial}{\partial t}+\boldsymbol{v}\cdot\nabla\right)\delta\wp\left(\boldsymbol{r},\boldsymbol{v},t\right)\\&=\int \mathrm{d}\boldsymbol{r}'\mathrm{d}\boldsymbol{v}'\Gamma(\boldsymbol{r},\boldsymbol{v},\boldsymbol{r}',\boldsymbol{v}')\delta\wp(\boldsymbol{r}',\boldsymbol{v}',t),\end{aligned}\tag{1}$$

where t denotes time, $\boldsymbol{r}$ and $\boldsymbol{v}$ are the coordinate and velocity of fluid particles, respectively. In addition, $\wp(\boldsymbol{r},\boldsymbol{v},t)$ represents the singlet distribution function in the dynamics of the inhomogeneous fluid, while $\delta\wp$ denotes the deviation from its equilibrium value. The involved quality $\Gamma(\boldsymbol{r},\boldsymbol{v},\boldsymbol{r}',\boldsymbol{v}')$ is related to the frequency matrix that reflects the instantaneous response within the system. Its complex and obscure expression can be found in the literature.[20]

Further, assuming that in the dynamics, the deviation of its density, velocity, temperature as well as the kinetic contributions to pressure tensor and energy flux are all small, it is safe to expand these continuum variables into Taylor series of the unit vector of the direction cosine, say $\hat{\boldsymbol{e}}$:

$$\begin{aligned}A(\boldsymbol{r}-\sigma\hat{\boldsymbol{e}},t)=&A(\boldsymbol{r},t)-\sigma\hat{\boldsymbol{e}}\cdot\nabla A(\boldsymbol{r},t)\\&+\frac{1}{2}\hat{\boldsymbol{e}}\hat{\boldsymbol{e}}:\nabla\nabla A(\boldsymbol{r},t)+\cdots,\end{aligned}\tag{2}$$

where $\hat{\boldsymbol{e}}=e_x\hat{i}+e_y\hat{j}+e_z\hat{k}$ with $e_x=\sin\theta\cos\phi$, $e_y=\sin\theta\sin\phi$, $e_z=\cos\theta$, and $A(\boldsymbol{r},t)$ stands for any of the above mentioned continuum variables.

With the aid of the 13-moment approximation,[24] a linearized Navier–Stokes equation for the energy transfer can

be obtained via some cumbersome calculation in the Fourier space, that is,

$$-\frac{3}{2}k_{\mathrm{B}}\mathrm{i}\omega\rho(\boldsymbol{r})\delta T(\boldsymbol{r},\omega)+\nabla\cdot\boldsymbol{J}(\boldsymbol{r},\omega)=R_{\mathrm{T}}(\boldsymbol{r},\omega) \tag{3}$$

with k_{B} being the Boltzmann constant and ω the frequency. Here, $\boldsymbol{J}(\boldsymbol{r},\omega)$ is the time Fourier transform of the energy flux, while $R_{\mathrm{T}}(\boldsymbol{r},\omega)$ denotes the corresponding thermodynamic source. For the sake of brevity, the explicit expressions for $\boldsymbol{J}(\boldsymbol{r},\omega)$ and $R_{\mathrm{T}}(\boldsymbol{r},\omega)$ are not presented here, and the interested reader can refer to the literature.[20,21] Performing the spatial differentiation on both sides, and gathering the terms of the form $-\hat{\lambda}\cdot\delta T(\boldsymbol{r},\omega)$, with $\hat{\lambda}$ denoting the second rank thermal conductivity tensor, one can obtain the local thermal conductivity of the inhomogeneous fluids.

Specifically, in the limit of zero frequency, the PG expression for the normal component of the thermal conductivity in a slit pore can be given as[20]

$$\lambda_{\mathrm{PG}}(z)=\lambda_0\rho(z)[\lambda_1(z)+\lambda_2(z)]. \tag{4}$$

Here, $\lambda_0=75k_{\mathrm{B}}/(64\sigma^2\sqrt{\pi\beta m})$ is the thermal conductivity of the dilute gas, with σ and m representing the diameter and mass of the particle, respectively. In addition, $\beta=1/(k_{\mathrm{B}}T)$ with T being the absolute temperature. In Eq. (4), $\lambda_1(z)$ and $\lambda_2(z)$ stand for contributions arising from the isotropic and anisotropic components of energy flux, respectively. Their explicit expression can be given as

$$\lambda_1(z)=4\pi\tau(z)\left[1+\frac{9b}{20}\chi(z)\right]^2+\frac{24b^2}{25\pi}\chi(z), \tag{5a}$$

$$\lambda_2(z)=\frac{9\pi b}{5}\tau(z)\xi(z)\left[2+\frac{9b}{10}\chi(z)+\frac{9b}{20}\xi(z)\right]+\frac{24b^2}{25\pi}\xi(z), \tag{5b}$$

with $b=2\pi\sigma^3/3$ being the second virial coefficient of the dilute gas. Moreover, the involved auxiliary functions in Eq. (5) are respectively defined as

$$\chi(z)=\frac{1}{\sigma^3}\int_{z-\sigma}^{z+\sigma}\mathrm{d}z'[\sigma^2-(z-z')^2]\rho(z')g_{\mathrm{c,ff}}^{\mathrm{inh}}(z,z'|\rho,T), \tag{6a}$$

$$\xi(z)=\frac{1}{\sigma^3}\int_{z-\sigma}^{z+\sigma}\mathrm{d}z'[3(z-z')^2-\sigma^2]\rho(z')g_{\mathrm{c,ff}}^{\mathrm{inh}}(z,z'|\rho,T), \tag{6b}$$

$$\tau(z)=\frac{1}{2\pi}[\nu(z)-\frac{27}{32}\nu_1(z)-\frac{13\sqrt{2}}{8}\nu_2(z)]^{-1}, \tag{6c}$$

$$\nu(z)=\frac{1}{\sigma}\int_{z-\sigma}^{z+\sigma}\mathrm{d}z'\rho(z')g_{\mathrm{c,ff}}^{\mathrm{inh}}(z,z'|\rho,T), \tag{6d}$$

$$\nu_1(z)=\frac{1}{\sigma}\int_{z-\sigma}^{z+\sigma}\mathrm{d}z'[\rho(z')-\rho(z)]g_{\mathrm{c,ff}}^{\mathrm{inh}}(z,z'|\rho,T), \tag{6e}$$

$$\nu_2(z)=\frac{1}{\sigma_{\mathrm{sf}}}\int_{z-\sigma_{\mathrm{sf}}}^{z+\sigma_{\mathrm{sf}}}\mathrm{d}z'\rho(z')g_{\mathrm{c,sf}}^{\mathrm{inh}}(z,z'|\rho,T). \tag{6f}$$

Note that the above equations are different in forms from those given by PG, since the involved integrals have been transformed from the angular space to the coordinate space. Moreover, in the bulk limit, the PG result, say Eq. (4), recovers exactly the MFT result for the homogeneous fluid,[24] that is,

$$\lambda_{\mathrm{MFT}}^{\mathrm{hom}}(\rho_{\mathrm{b}},T)=\lambda_0\left\{\frac{1}{g_{\mathrm{c,ff}}^{\mathrm{hom}}(\rho_{\mathrm{b}},T)}\left[1+\frac{3}{5}\rho_{\mathrm{b}}bg_{\mathrm{c,ff}}^{\mathrm{hom}}(\rho_{\mathrm{b}},T)\right]^2+\frac{32}{25\pi}\rho_{\mathrm{b}}^2b^2g_{\mathrm{c,ff}}^{\mathrm{hom}}(\rho_{\mathrm{b}},T)\right\}, \tag{7}$$

with ρ_{b} being the bulk density of the homogeneous fluid. Note that in this case, the radial distribution function at contact $g_{\mathrm{c,ff}}^{\mathrm{hom}}(\rho_{\mathrm{b}},T)$ is independent of position, but relies on density as well as temperature. For simplicity in the calculations, $g_{\mathrm{c,ff}}^{\mathrm{hom}}(\rho_{\mathrm{b}},T)$ can be determined by the analytical result proposed by Johnson *et al.*,[25] that is,

$$g_{\mathrm{c,ff}}^{\mathrm{hom}}(\rho_{\mathrm{b}}^*,T^*)=1+\sum_{i,j=1}^{5}a_{ij}\rho_{\mathrm{b}}^{*i}T^{*(1-j)}. \tag{8}$$

In this equation, the dimensionless qualities have been defined, i.e., $\rho_{\mathrm{b}}^*=\rho_{\mathrm{b}}\sigma^3$, $T^*=k_{\mathrm{B}}T/\varepsilon$ with ε being the potential strength. The combination parameters a_{ij} can be found in the literature.[25]

It is necessary to emphasize that in Eqs. (6a)–(6f), both $g_{\mathrm{c,ff}}^{\mathrm{inh}}(z,z'|\rho,T)$ and $g_{\mathrm{c,sf}}^{\mathrm{inh}}(z,z'|\rho,T)$ are the radial distribution functions at contact in inhomogeneous fluid. Take $g_{\mathrm{c,ff}}^{\mathrm{inh}}(z,z'|\rho,T)$ as an example, it describes the probability of the situation in which one particle locates at z and another particle locates simultaneously at z', with their centroid distance being σ. In order to include the correlation effect in the inhomogeneous fluid, the involved density in $g_{\mathrm{c,ff}}^{\mathrm{inh}}(z,z'|\rho,T)$ can be regarded as the algebraic average of the local densities at z and z'. In this work, we set it as $\tilde{\rho}(z,z')=\frac{1}{2}[\bar{\rho}(z)+\bar{\rho}(z')]$. Accordingly, it can be obtained as

$$g_{\mathrm{c,ff}}^{\mathrm{inh}}(z,z'|\rho,T)=g_{\mathrm{c,ff}}^{\mathrm{hom}}(\tilde{\rho}(z,z'),T). \tag{9}$$

Note that $\bar{\rho}(z)$ is the weighted density, whose explicit definition will be given in the following. In a similar way, the value of $g_{\mathrm{c,sf}}^{\mathrm{inh}}(z,z'|\rho,T)$ can also be determined.

3. Correlation contribution of the local thermal conductivity

As stated above, the PG theory places itself on an MFT level, which underestimates the correlation effect in the fluid. Actually, plenty of MD simulations have been performed to investigate the thermal conductivity of the bulk fluids. Based on the simulation results, some fitting expressions for bulk thermal conductivity have been proposed.[22,23] In the MD simulations, the correlation effect in fluids can be naturally taken into account in the simulation procedure. In this perspective, the simulation-based correlations should provide a feasible approach to consider the correlation contribution of the thermal conductivity. In view that the MFT contribution has been taken into account in the PG theory, one need only extract from the simulation-based correlations the contribution that is beyond

the MFT level. By doing so, the thermal conductivity can be obtained as the summation of the PG result and the correlation contribution.

In this work, we employ the fitting result by Bugel and Galliero,[22] who expressed the reduced thermal conductivity, $\lambda^* \equiv \lambda \frac{\sigma^2}{k_B}\sqrt{\frac{m}{\varepsilon}}$, of the bulk LJ fluid as

$$\lambda^{*\mathrm{hom}}_{\mathrm{sim}}(\rho^*_{\mathrm{b}}, T^*) = \lambda^*_{\mathrm{k}}(T^*) + \lambda^*_{\mathrm{r}}(\rho^*_{\mathrm{b}}, T^*) + \lambda^*_{\mathrm{c}}(\rho^*_{\mathrm{b}}, T^*), \quad (10)$$

where $\lambda^*_{\mathrm{k}} = \frac{75}{64\Omega_V}\sqrt{\frac{T^*}{\pi}}$ is the reduced kinetic contribution with the collision integral Ω_V. In addition, λ^*_{r} and λ^*_{c} are residual contribution and an enhancement due to the proximity of the critical point, respectively. Their explicit expressions are

$$\lambda^*_{\mathrm{r}}(\rho^*_{\mathrm{b}}, T^*) = A(T^*)\left[\exp\left[B(T^*)\rho^{*\frac{2}{3}}_{\mathrm{b}}\right] - 1\right], \quad (11a)$$

$$\lambda^*_{\mathrm{c}}(\rho^*_{\mathrm{b}}, T^*) = a(T^*\rho^{*2}_{\mathrm{b}}\chi^*_{\mathrm{T}})^b. \quad (11b)$$

In Eq. (11a), the two temperature-dependent factors are defined as $A(T^*) = cT^* + d$ and $B(T^*) = eT^* + f$. Moreover, $\chi^*_{\mathrm{T}} \equiv \chi_{\mathrm{T}}\frac{\varepsilon}{\sigma^3}$ is the reduced isothermal compressibility and the fitting parameters a–f can be found in the literature.[22]

According to the proposal stated above, the correlation contribution of thermal conductivity in the bulk LJ fluids can be first obtained by subtracting $\lambda^{\mathrm{hom}}_{\mathrm{MFT}}$ in Eq. (7) from $\lambda^{\mathrm{hom}}_{\mathrm{sim}}$, that is,

$$\lambda^{\mathrm{hom}}_{\mathrm{cor}}(\rho_{\mathrm{b}}, T) = \lambda^{\mathrm{hom}}_{\mathrm{sim}}(\rho_{\mathrm{b}}, T) - \lambda^{\mathrm{hom}}_{\mathrm{MFT}}(\rho_{\mathrm{b}}, T). \quad (12)$$

Having obtained the correlation contribution in the bulk fluid, one would like to generalize it to the case of inhomogeneous fluid. In the generalization, the concept of WDA is borrowed from the DFT calculation for the equilibrium properties in confined fluid. Accordingly, the involved ρ_{b} in Eq. (12) should be replaced by a weighted density $\bar{\rho}(z)$, rather than the local density $\rho(z)$. Then, the local correlation contribution can be obtained as follows:

$$\lambda^{\mathrm{loc}}_{\mathrm{cor}}(z) = \lambda^{\mathrm{hom}}_{\mathrm{cor}}(\bar{\rho}(z), T). \quad (13)$$

Here, the weighted density is defined as $\bar{\rho}(z) = \int \rho(z')\omega_1(|z'-z|)\mathrm{d}z'$, with the weight function $\omega_1(|z'-z|) = \frac{3}{4s_1^2}[s_1^2 - (z'-z)^2]$. Evidently, the combination of Eqs. (4) and (13) provides a scheme for the local thermal conductivity in the inhomogeneous fluids. This is referred as a PG+WDA1 scheme in the following.

Nevertheless, as illustrated by Hoang *et al.*[26] in their investigation on the shear viscosity of confined fluids, the traditional weight function developed for the static properties is inadequate to provide an accurate estimation of the dynamic properties, and more kinetic correlation should be taken into account. To overcome this limitation, they proposed a specific weighted density by considering the momentum exchange between the colliding particles. The key point in their complicated calculation is how to identify the position where the local property is defined. This is physically in line with Percus's idea for the coarse-grained free energy density of the inhomogeneous fluids.[27] Unlike their treatments, this work adopts an alternative route by performing a further smooth procedure on the local value of $\lambda^{\mathrm{loc}}_{\mathrm{cor}}(z)$, that is,

$$\lambda_{\mathrm{cor}}(z) = \int \lambda^{\mathrm{loc}}_{\mathrm{cor}}(z')\omega_2(|z'-z|)\mathrm{d}z', \quad (14)$$

with $\omega_2(|z'-z|) = \frac{3}{4s_2^2}[s_2^2 - (z'-z)^2]$ being another weight function. Accordingly, the final results for the local thermal conductivity in an inhomogeneous fluid read

$$\lambda(z) = \lambda_{\mathrm{PG}}(z) + \lambda_{\mathrm{cor}}(z). \quad (15)$$

For the purpose of differentiation, Eq. (15) is referred as a PG+WDA2 scheme. It should be noted that the difference between the two weight functions, say $\omega_1(|z'-z|)$ and $\omega_2(|z'-z|)$, lies in the region in which the weighted average is performed, and that the parameters s_1 and s_2 are unnecessarily identical. Yet, it is found that the values of $s_1 = s_2 = 0.8\sigma$ can produce satisfactory results in the calculation.

4. DFT scheme for confined LJ fluids

In this study, we focus on the thermal conductivity of argon film that is confined in the slit pore. For convenience, the argon-argon pair interaction is modeled by the LJ potential, which reads

$$\varphi(r) = 4\varepsilon\left[\left(\frac{\sigma}{r}\right)^{12} - \left(\frac{\sigma}{r}\right)^{6}\right]. \quad (16)$$

For a confined fluid that is equilibrium with a reservoir, its equilibrium structure can be determined by classical DFT.[28,29] In the framework of DFT, the equilibrium density, say $\rho(z)$, can be calculated via the variation of grand potential functional $\Omega[\rho(z)]$ with respect to $\rho(z)$ at constant chemical potential, volume and temperature, that is,

$$\frac{\delta}{\delta\rho(z)}\Omega[\rho(z)] = 0. \quad (17)$$

In grand canonical ensemble, the grand potential functional $\Omega[\rho(z)]$ is given as

$$\Omega[\rho(z)] = F[\rho(z)] + \int \mathrm{d}z\rho(z)[V_{\mathrm{ext}}(z) - \mu], \quad (18)$$

with μ and $V_{\mathrm{ext}}(z)$ being chemical potential and external potential, respectively. Evidently, the key point in the DFT calculation is to construct the intrinsic Helmholtz free enregy functional $F[\rho(z)]$. Usually, it can be perturbatively decomposed into several contributions. For the LJ fluid under consideration, it reads

$$F[\rho(z)] = F_{\mathrm{id}}[\rho(z)] + F_{\mathrm{hs}}[\rho(z)] + F_{\mathrm{att}}[\rho(z)] \quad (19)$$

with the three terms on the rhs represent contributions from ideal gas, hard sphere and long-ranged attraction, respectively.

Among them, $F_{\rm id}[\rho(z)]$ can be exactly obtained by formal calculation, and $F_{\rm hs}[\rho(z)]$ can be well treated by the modified fundamental measure theory (MFMT).[30,31] Moreover, the attractive contribution $F_{\rm att}[\rho(z)]$ can be appropriately expressed via either the weighted density approximation (WDA)[32,33] or a functional Taylor expansion.[34,35] Both treatments have achieved satisfied performance in investigations on diverse aspects of confined fluids. In this work, the WDA method is employed. For the purpose of concise, more details about MFMT and WDA can refer to the literature.[36,37]

5. Numerical results and discussion

To check the performance of the proposed methods in this work, we have calculated the overall thermal conductivity, say $\lambda_{\rm av}$, by performing a harmonic average of its inhomogeneous profile in the pore:

$$\lambda_{\rm av} = \left[\frac{1}{H-2\delta}\int_{\delta}^{H-\delta}\lambda^{-1}(z)\,{\rm d}z\right]^{-1}. \tag{20}$$

Here the parameter δ is introduced because the fluid particle is prevented from entering the region that is adjacent to the pore wall.[38] As a test, $\lambda_{\rm av}$ of liquid argon confined in krypton slit pore is calculated. The potential from each pore wall is described by the 10 and 4 potential:

$$w(z) = 2\pi\varepsilon_{\rm sf}\rho_{\rm s}\sigma_{\rm sf}^2\left[\frac{2}{5}\left(\frac{\sigma_{\rm sf}}{z}\right)^{10} - \left(\frac{\sigma_{\rm sf}}{z}\right)^{4}\right]. \tag{21}$$

Accordingly, the external potential can be obtained as $V_{\rm ext}(z) = w(z) + w(H-z)$. Note that the values of the model parameters are set the same as those used in the simulation:[15] $\sigma = 0.3405$ nm, $\sigma_{\rm sf} = 0.3519$ nm, $\varepsilon/k_{\rm B} = 119.8$ K, $\varepsilon_{\rm sf}/k_{\rm B} = 141.4$ K, and $\rho_{\rm s} = 5.5095$ nm^2.

Figure 1(a) depicts the pore-size dependence of $\lambda_{\rm av}$ for confined liquid argon under the conditions of $\rho_{\rm b}^* = 0.642$ and $T^* = 1.0$. To display the superiority of the PG+WDA2 scheme over other methods, the results from PG+WDA1, PG, and LADM[38] methods are also given in the figure. Note that the reduced pore width $H^* = H/\sigma$ is defined here. Comparison between results from different methods suggests that for $\lambda_{\rm av}$ of the confined argon, the PG+WDA2 scheme reproduces the MD results[15] very well. In contrast, both the PG+WDA1 and LADM methods overestimate the value of $\lambda_{\rm av}$, while the PG method underestimates its value. This provides strong evidence for the discrepancy in treating the static and dynamic properties of the confined fluids, and for the necessity of performing the second weighted average in Eq. (14).

Moreover, it is obvious that in the pores with different widths, the value of $\lambda_{\rm av}$ is usually smaller than those of the bulk fluids. This arises from the ordered layer structure that formed in the pore, especially in the regions near the walls. The particle layers are so closely arranged that they prevent the energy flowing caused by the particle translation. This can be confirmed by the results shown in Fig. 1(b), which gives the spatial profiles of fluid density and thermal conductivity in a pore of $H^* = 12.0$. The results in Fig. 1(b) also show that $\lambda(z)$ is nearly in phase with $\rho(z)$. However, the first crest near the wall is small, while the second crest displays a maximal peak. Actually, Rah and Eu[39] have decomposed λ into contributions from kinetics, configuration and stress work. Among them, contributions from kinetics and stress work rely on the movement of atom in the pore, while the configurational contribution depends mainly on the inter-atom interaction. In term of this, the maximal peak of $\lambda(z)$ near the second atom layer can be interpreted by the strong interaction felt by the atom there.

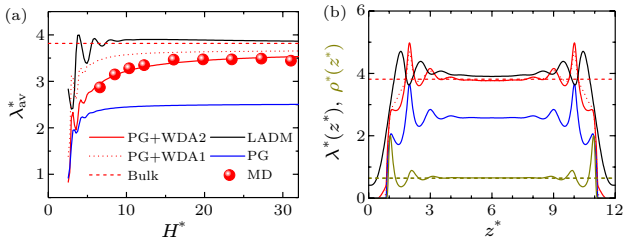


Fig. 1. (a) Dependence of $\lambda_{\rm av}$ of confined liquid argon on the pore width H^*. The red dashed line stands for the bulk thermal conductivity. (b) Profiles of $\lambda^*(z^*)$ in the pore of a width of $H^* = 12.0$. The solid green line represents $\rho^*(z^*)$, the dashed red line and dashed green line stand for the bulk thermal conductivity and bulk density, respectively. The other lines are the profiles of $\lambda^*(z^*)$ obtained from different methods, which take the same line types as those given in (a). Moreover, all the calculations are performed under the conditions of $\rho_{\rm b}^* = 0.642$ and $T^* = 1.0$.

Further, in each set of results in Fig. 1(a), an oscillatory increment of $\lambda_{\rm av}^*$ with H^* can be observed when H^* is small. This is also due to the formation of layer structure in the pore. As stated above, the layer structure is detrimental to the particle translation. However, a further increment of H^* may loosen the particle layer and then enhances the energy flowing, until a new particle layer is formed. When H^* is large enough, the two walls decouple, and only two thin layers are formed due to the adsorption of the separated walls. In this instance, the layer structure keeps unchanged in the region near the walls, and then the substantial modulation of $\lambda_{\rm av}^*$ by the layer structure disappears.

In order for further understanding about the physics of the method proposed in Eq. (15), it is necessary to clarify the extent to which the confinement can influence the PG and correlation contributions. To this end, the PG and correlation contributions of $\lambda^*(z^*)$ of the confined liquid argon are calculated under the conditions of $T^* = 1.5$ and $H^* = 6.0$. The results are given in Fig. 2. It is evident that $\lambda_{\rm PG}^*(z^*)$ shows obvious oscillation due to the confinement arising from the pore. Moreover, the oscillation of $\lambda_{\rm PG}^*(z^*)$ turns more violent with the increase of $\rho_{\rm b}^*$. On the contrary, the correlation contribution $\lambda_{\rm cor}^*(z^*)$ exhibits rather weak oscillation in the central region of the pore. However, in the region near the walls, $\lambda_{\rm cor}^*(z^*)$ is depressed

as it is approaching the walls. This can be understood by the formation of the adsorption layer near the walls. Furthermore, comparison between the values of $\lambda^*_{\rm PG}(z^*)$ and $\lambda^*_{\rm cor}(z^*)$ suggests that $\lambda^*_{\rm cor}(z^*)$ can play a non-negligible role, especially in the case of larger $\rho^*_{\rm b}$.

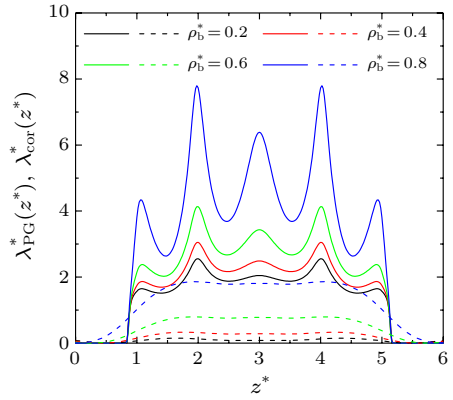


Fig. 2. The PG and correlation contributions of $\lambda^*(z^*)$ of liquid argon confined in slit pore. In the calculation, the parameters are set as $T^*=1.5$ and $H^*=6.0$. The solid and dashed lines stand for the results of $\lambda^*_{\rm PG}(z^*)$ and $\lambda^*_{\rm cor}(z^*)$, respectively.

5.1. Effect of fluid parameters on the local thermal conductivity

In the confined fluidic film, the local structure plays a decisive role in determining its static properties. This is also true for the thermal conductivity, as suggested by its density dependence in Eq. (4). Actually, most of the reported investigations focus on the overall thermal conductivity of the confined fluids, while little is known about its local profile in the pore. From a microscopic point of view, knowledge of the local thermal conductivity is crucial to deepen our understanding about the thermal transfer in the confined fluids. Thus, it is necessary to calculate the inhomogeneous profile of thermal conductivity in the pore, and to analyze its dependence on different influence factors. In this section, our attention is focused on the influence of fluid parameters, i.e., the bulk density and the temperature.

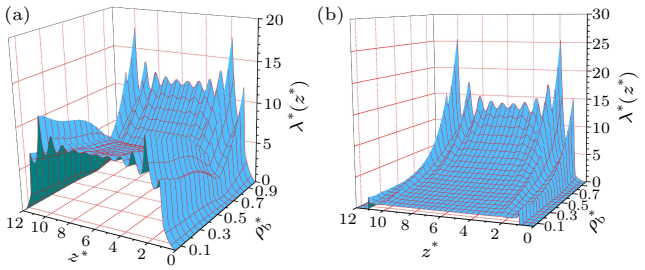


Fig. 3. Inhomogeneous profiles of $\lambda^*(z^*)$ under different conditions of $\rho^*_{\rm b}$. (a) $T^*=0.7$ and (b) $T^*=2.0$. In the calculations, the pore parameters are set as $H^*=12.0$ and $\varepsilon_{\rm sf}/\varepsilon=1.18$.

In Fig. 3, the effect of bulk density on the local thermal conductivity is given. In this figure, the calculations are performed under the conditions of $H^*=12.0$ and $\varepsilon_{\rm sf}/\varepsilon=1.18$. Moreover, in order to understand the thermal conductivity of confined fluids in different phase states, two different temperatures have been chosen. They are $T^*=0.7$ and $T^*=2.0$, both of which are far enough from the LJ critical temperature $T^*_{\rm c}\sim 1.31$. Figure 3(a) shows that in the subcritical case, $\lambda^*(z^*)$ undergoes a decrease-increase transition with the increment of $\rho^*_{\rm b}$. This can be attributed to the occurrence of capillary condensation at the low temperature. Physically, the capillary condensation is a gas-liquid transition occurring at a pressure lower than the saturation pressure. When the condensation of a gas phase takes place in the pore, the formed liquid bridge takes the density of its coexisting liquid phase. According to the gas-liquid phase equilibrium, for the given temperature, the smaller the gas density, the larger its coexisting liquid density. Therefore, when $\rho^*_{\rm b}$ is very small, the thermal conductivity is reduced with a further increment of $\rho^*_{\rm b}$. In contrast, the condition is different when $\rho^*_{\rm b}$ is large enough. It is shown that for $\rho^*_{\rm b}>0.6$, the capillary condensation is absent, and $\lambda^*(z^*)$ increases monotonically with $\rho^*_{\rm b}$. This can be explained by the positive correlation of thermal conductivity with density, as indicated in Eqs. (4) and (15).

Figure 3(b) is calculated at a supercritical temperature $T^*=2.0$. Unlike the case in Fig. 3(a), the thermal conductivity in Fig 3(b) increases monotonically with $\rho^*_{\rm b}$ in the whole region of $\rho^*_{\rm b}$. When $\rho^*_{\rm b}$ is small, $\lambda^*(z^*)$ takes a typical gaseous value in the central region of the pore, while it exhibits two visible peaks in the region near the walls. Actually, these peaks arise from the adsorption by the walls. As $\rho^*_{\rm b}$ is increased, several crests continuously appear in the curve. This results again from the layer structure in the pore. Further, by comparing the results in the cases of small and large $\rho^*_{\rm b}$, it is interesting to find that when $\rho^*_{\rm b}$ is large, the first crest next to the wall is smaller than the second one; when $\rho^*_{\rm b}$ is small, the first crest is larger. This can be understood by the different roles played by the formed particle layer in these two cases. In the former case, a larger $\rho^*_{\rm b}$ leads to a denser particle layer, which prevent the energy from flowing via particle translation. Nevertheless, in the latter case, the adsorbed particle layer is not dense enough to prevent the particle from translating. Instead, it is conducive to the configurational contribution of the thermal conductivity.

In order to understand the influence of temperature on the local thermal conductivity of the confined fluids, the dependence of $\lambda^*(z^*)$ on T^* is calculated under the conditions of $H^*=12.0$ and $\varepsilon_{\rm sf}/\varepsilon=1.0$. In the calculations, two distinct densities, i.e., $\rho^*_{\rm b}=0.1$ and $\rho^*_{\rm b}=0.8$, are set to show the effect of capillary condensation occurred in the cases of low temperature and small density. The corresponding results are given in Figs. 4(a) and 4(b), respectively.

Figure 4(a) shows the temperature dependence of $\lambda^*(z^*)$ in the case of $\rho^*_{\rm b}=0.1$. In this figure, the results of $\lambda^*(z^*)$ in the low temperature region are in stark contrast to those in the high temperature region. For the chosen values of parameters,

the turning point locates nearly at $T^* \sim 1.25$. Such a sharp contrast implies that the temperature dependence of $\lambda^*(z^*)$ has been ruled by different mechanisms in different temperature regions. In the region of $T^* > 1.25$, $\lambda^*(z^*)$ exhibits the typical gaseous value in the central region of the pore, and it shows a tenuous increment with T^*. This is because the kinetic contribution of $\lambda^*(z^*)$ is dominant, and the enhanced thermal motion of fluid particle is helpful for the energy flowing. Even so, two conspicuous peaks are still observed in the immediate neighborhood of the walls, due to the adsorption of the fluid particles there. In contrast, in the region of $T^* < 1.25$, $\lambda^*(z^*)$ is significantly larger than that of the bulk fluid. Meanwhile, with the decrease of T^*, it grows larger and both the value and amplitude of its oscillation are enhanced. This can be interpreted by the capillary condensation in the pore, which occurs usually at a low temperature. Specifically, for the given gaseous bulk density, the lower the temperature is, the larger the density of the condensed liquid film is.

In Fig. 4(b), the dependence of $\lambda^*(z^*)$ on T^* in the case of $\rho_b^* = 0.8$ is depicted. The results suggest that for the given ρ_b^*, $\lambda^*(z^*)$ increases monotonically with T^*. This is identical to the trend shown in the cases of low density and high temperature, but exactly opposite to that in the cases of low density and low temperature, which has been discussed in Fig. 4(a).

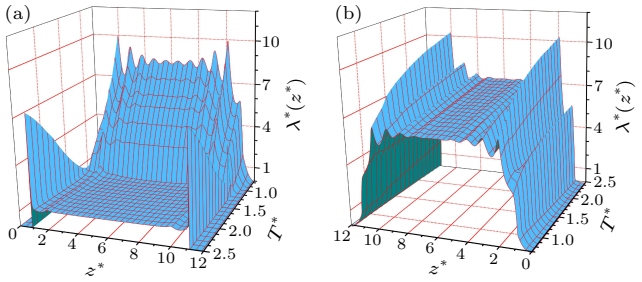


Fig. 4. Inhomogeneous profiles of $\lambda^*(z^*)$ under different conditions of T^*: (a) $\rho_b^* = 0.1$, (b) $\rho_b^* = 0.8$. In the calculations, the pore parameters are set as $H^* = 12.0$ and $\varepsilon_{sf}/\varepsilon = 1.0$.

5.2. Effect of pore parameters on the local thermal conductivity

In the above subsection, the effect of fluid parameters, i.e., ρ_b^* and T^*, on the local thermal conductivity of the nano-fluidic films has been studied. Actually, besides these fluid characteristics, the pore characteristics can also modulate the structure of the confined fluids. In the light of the correlation between thermal conductivity and density, it is expected that the structural modulation by the confinement can be passed on to the thermal conductivity of the film. In this subsection, therefore, the influences of pore width and potential strength on the thermal conductivity are investigated.

The dependence of $\lambda^*(z^*)$ on the pore width H^* is given in Fig. 5. In the calculations, we have set $T^* = 1.5$ and $\varepsilon_{sf}/\varepsilon = 1.0$, while the bulk densities are set as $\rho_b^* = 0.1$ and $\rho_b^* = 0.8$ in Figs. 5(a) and 5(b), respectively. It is interesting that in Fig. 5(a), the thermal conductivity of the nano-fluidic film is liquid-like when $H^* < 5.0$, while it decays gradually to a gas-like one with the increment of H^*. This attributes again to the occurrence of capillary condensation in the narrower pore. In other words, when the pore is narrow, the two walls are so close that the superposition of their potentials enhances extremely the adsorption in the pore, though the temperature is higher than the critical temperature $T_c^* \sim 1.31$. Therefore, it follows that the confinement of the pore can raise the critical temperature at which the capillary condensation occurs. However, when H^* is large enough, the pore decouples into two irrelevant walls, which leads to the appearance of gaseous phase in the central region of the pore.

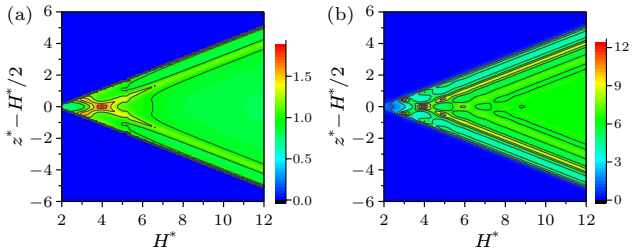


Fig. 5. Contour plot of $\lambda^*(z^*)$ under different conditions of H^*: (a) $\rho_b^* = 0.1$, (b) $\rho_b^* = 0.8$. In the calculations, the other parameters are set as $T^* = 1.5$ and $\varepsilon_{sf}/\varepsilon = 1.0$.

Figure 5(b) depicts the dependence of $\lambda^*(z^*)$ on H^* in the case of $\rho_b^* = 0.8$. In this situation, $\lambda^*(z^*)$ keeps liquid-like as H^* is varied. In addition, some microscopic information about the geometric modulation has been clearly displayed. It is obvious that the number of crests appearing in the curves relies heavily on the pore width. During the increment of H^*, the new crest emerges in the curve whenever H^* takes nearly an integer. From a physical perspective, this is decided by the structural modulation of the confined fluid and can be understood by the correlation between $\lambda^*(z^*)$ and $\rho^*(z^*)$. When H^* is exactly capable of accommodating integer layers of fluid particles, a well-arranged layer structure is formed in the pore. Further increment of H^* will relax the packed structure, until a new well-arranged layer structure is reformed. This also explains why a variation of nearly one diameter is required to introduce a new crest in the curve of $\lambda^*(z^*)$. The results in the figure also suggest that when $H^* > 9.0$, no new crest appears as H^* is further increased. This is because the decoupled two walls can not modulate the fluid structure anymore, and the fluid in the central region of the pore maintains the bulk density ρ_b^*.

For the confined fluid under consideration, the adsorption potential from the walls imposes a direct impact on the fluid structure and then on the thermal conductivity. Thus, it is necessary to investigate the effect of the potential strength, say ε_{sf}, on $\lambda^*(z^*)$. The relevant results are given in Fig. 6. In the calculations, the temperature is kept at $T^* = 1.5$, and the

pore width is set as $H^* = 6.0$ in order to highlight the influence of ε_{sf}. Moreover, the bulk densities are set as $\rho_b^* = 0.1$ and $\rho_b^* = 0.8$ in Figs. 6(a) and 6(b), respectively. In Fig. 6(a), it is evident that when $\varepsilon_{sf}/\varepsilon$ is small, the confined fluid exhibits a gas-like thermal conductivity in the central region of the pore, but with a striking peak near each wall. This is just the expected because the weak adsorption potential imposes only a negligible influence to the fluid. However, the situation becomes extremely different when $\varepsilon_{sf}/\varepsilon$ is large. On the one hand, with the increment of $\varepsilon_{sf}/\varepsilon$, a liquid-like thermal conductivity is exhibited in the central region of the pore. On the other hand, the oscillation of $\lambda^*(z^*)$ turns more violent as $\varepsilon_{sf}/\varepsilon$ is increased. In these situations, the adsorption potential is so strong that it can give rise to capillary condensation, which is responsible for the enhancement of $\lambda^*(z^*)$ in the pore. Together with the results shown in Fig. 5(a), a conclusion can be safely drawn that both smaller H^* and larger $\varepsilon_{sf}/\varepsilon$ are conducive to the enhancement of $\lambda^*(z^*)$ of the confined fluid. In contrast to the complex modulation in the case of $\rho_b^* = 0.1$, Fig. 6(b) suggests that in a confined fluid with $\rho_b^* = 0.8$, the variation of $\varepsilon_{sf}/\varepsilon$ applies only a monotonous modulation on the profile of $\lambda^*(z^*)$, i.e., the stronger the adsorption potential is, the larger the thermal conductivity and its oscillation amplitude are.

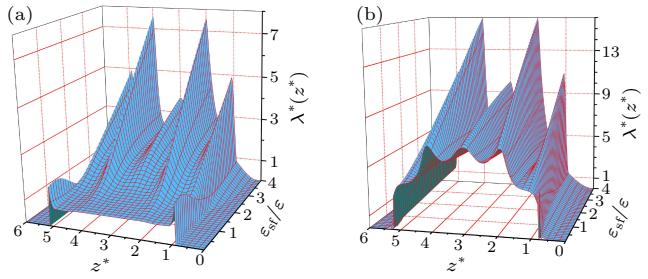


Fig. 6. Inhomogeneous profiles of $\lambda^*(z^*)$ under different conditions of $\varepsilon_{sf}/\varepsilon$: (a) $\rho_b^* = 0.1$, (b) $\rho_b^* = 0.8$. In the calculations, the pore parameters are set as $H^* = 6.0$ and $T^* = 1.5$.

6. Overall thermal conductivity of the nano-fluidic film

In the above two sections, the inhomogeneous profile of thermal conductivity in the nano-fluidic films has been focused. Though the inhomogeneous thermal conductivity is helpful to understand the thermal transfer from a microscopic perspective, it is usually inaccessible in most of the experimental measurements. On the contrary, it is more convenient to measure the thermal conductivity of the confined fluid as a whole. To this end, this section focuses the overall thermal conductivity λ_{av}^* of the fluidic film, which has been defined in Eq. (20). In order to gain a comprehensive understanding about λ_{av}^*, effects of both fluid parameters and pore parameters are calculated and investigated, just as done for the local thermal conductivity $\lambda^*(z^*)$.

In Fig. 7, the effects of fluid parameters, i.e., ρ_b^* and T^*, on the overall thermal conductivity are given. In these calculations, the pore width is set as $H^* = 6.0$, while the potential strength is set as $\varepsilon_{sf}/\varepsilon = 1.18$ and $\varepsilon_{sf}/\varepsilon = 3.0$ in Figs. 7(a) and 7(b), respectively. In Fig. 7(a), the results suggest that λ_{av}^* behaves differently in different phase regions. First, the value of λ_{av}^* in the region of small ρ_b^* and small T^* is prominently larger than that in the region of small ρ_b^* and large T^*. This is the result of the occurrence of capillary condensation at the lower temperature. Second, in the region of large ρ_b^*, λ_{av}^* shows a weak correlation with the temperature, which is consistent with the results in Fig. 4(b). This is in sharp contrast to the case of small ρ_b^*, in which λ_{av}^* is strongly correlated with the temperature. Third, in the region of small ρ_b^* and large T^*, the sparsely distributed contour lines suggest that in this phase region, λ_{av}^* depends slightly on either ρ_b^* or T^*. This can be attributed to the dominance of the kinetic contribution in the thermal conductivity of the dilute gas. In addition, Fig. 7(b) plots the result of λ_{av}^* under the condition of $\varepsilon_{sf}/\varepsilon = 3.0$. It is obvious that the pattern of contour line distribution is similar to that in Fig. 7(a), except that the region where capillary condensation occurs is enlarged along both the ρ_b^* and T^* axes. This is because the stronger potential has enhanced the coupling of the two walls, which raises both the critical density and the critical temperature for the occurrence of capillary condensation.

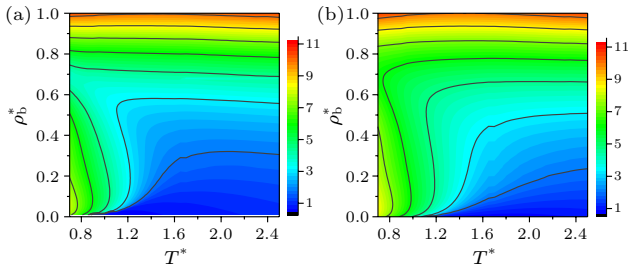


Fig. 7. Contour plot of λ_{av}^* under different conditions of ρ_b^* and T^*: (a) $\varepsilon_{sf}/\varepsilon = 1.18$, (b) $\varepsilon_{sf}/\varepsilon = 3.0$. In these calculations, the pore width is set as $H^* = 6.0$.

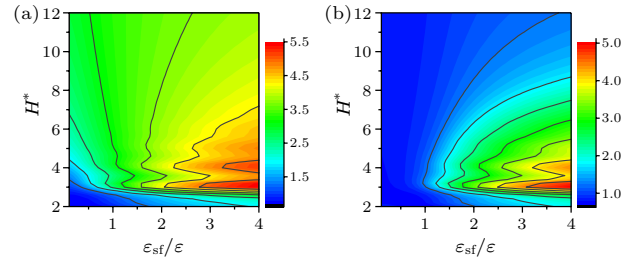


Fig. 8. Contour plot of λ_{av}^* under different conditions of H^* and $\varepsilon_{sf}/\varepsilon$: (a) $\rho_b^* = 0.6$, (b) $\rho_b^* = 0.1$. In the calculations, the temperature is set as $T^* = 1.5$.

In Fig. 8, the effects of pore parameters, i.e., H^* and $\varepsilon_{sf}/\varepsilon$, on the overall thermal conductivity λ_{av}^* are displayed. In the calculations, the temperature is set as $T^* = 1.5$. In order to explore the underlying physics in different phase states, two different values of ρ_b^* have been set, i.e., $\rho_b^* = 0.6$ in Fig. 8(a) and

$\rho_b^* = 0.1$ in Fig. 8(b). As is expected, for an arbitrary value of H^*, the results in Fig. 8(a) show that λ_{av}^* can be continuously enhanced with the increment of $\varepsilon_{sf}/\varepsilon$. What is more, the enhancement is more significant in the narrower pores because the coupling between two closer walls is stronger. However, it is an exception for the pores with $H^* < 3.0$. This is because in this case, the fluid particles are arranged so orderly that they depress greatly the energy flowing via particle translation. In addition, it is evident that for the given value of $\varepsilon_{sf}/\varepsilon$, the curve of λ_{av}^* usually exhibits oscillation with H^*, and the oscillation is more violent for the larger value of $\varepsilon_{sf}/\varepsilon$. This is in line with the results shown in Fig. 1(a).

Figure 8(b) displays the results in the case of $\rho_b^* = 0.1$. In the case of small $\varepsilon_{sf}/\varepsilon$ or large H^*, the confined fluid exhibits a gas-like thermal conductivity because the confined fluid keeps gaseous. In contrast, in the case of large $\varepsilon_{sf}/\varepsilon$ or small H^*, the value of λ_{av}^* is dramatically enhanced. This can be attributed mainly to the occurrence of the capillary condensation, which may lead to a liquid-like thermal conductivity in the pore. Similar to the results in Fig. 8(a), the increment of $\varepsilon_{sf}/\varepsilon$ is naturally conducive to the thermal conductivity. However, for a given value of $\varepsilon_{sf}/\varepsilon$ that is large enough, the influence of H^* on λ_{av}^* is more complicated. The condition for the pore with $H^* < 3.0$ is similar to that shown in Fig. 8(a). With the increment of H^*, λ_{av}^* is enhanced by the capillary condensation in the pore; while for the pore with $H^* > 7.0$, λ_{av}^* regresses to a gas-like thermal conductivity because the capillary condensation has been depressed due to the decoupling of the two walls.

7. Conclusions

In this work, a novel method for the local thermal conductivity of the inhomogeneous fluid is proposed by combining the PG theory and the weighted density approximation. In this method, the PG theory measures the local thermal conductivity on a level of mean field, while the correlation effect that is beyond the mean field is treated by the weighted density approximation. The main ideas of the model and the underlying physics can be highlighted as follows:

(1) The inhomogeneous thermal conductivity in confined fluid is perturbatively decomposed into two contributions, i.e., the mean field PG part and the correlation part. Among them, the latter is firstly obtained by the simulation-based correlations, with the aid of the WDA treatment.

(2) The proposed PG+WDA2 scheme exhibits satisfying advantage over either the PG+WDA1 scheme or the LADM method. This provides solid evidence to confirm that the traditional WDA scheme developed for the static properties is inadequate to treat the dynamic properties.

(3) The dependence of the inhomogeneous thermal conductivity on the fluid and pore parameters reveals the microscopic mechanisms of determining the thermal energy transfer in confined fluids, especially the correlation between the variation of the thermal conductivity and the structural modulation in the pore.

Specifically, in its application to the fluidic film in slit pores, it is found that the thermal conductivity of film can be markedly modulated by the fluid and pore parameters. The main findings are as follows. Firstly, the results suggest that in the immediate neighborhood of the pore walls, the dependence of local thermal conductivity on the local density is not a simple positive correlation. This can be attributed to the closely arranged particle layer which inhibits the particle from traveling. Secondly, in the cases of low temperature, the profile of the local thermal conductivity exhibits a decrease-increase transition as the bulk density is increased, due to the occurrence of capillary condensation in the pore; while at a supercritical temperature, the thermal conductivity increases monotonically with the bulk density. Thirdly, the temperature shows different modulation patterns for the fluids with low and high bulk density. Specifically, the local thermal conductivity is monotonically increased with temperature when the bulk density is large. When the bulk density is small, it shows a decrease-increase transition as the temperature is increased. Fourthly, on the aspect of pore parameters, it is found that both the smaller pore width and the stronger adsorption potential are beneficial to the enhancement of the thermal conductivity, since both factors can raise the critical temperature at which the capillary condensation takes place.

In addition, it is also found that the overall thermal conductivity may be markedly different in different phase regions. This is the immediate result of the modulation of local thermal conductivity by these fluid and pore parameters. More interestingly, due to the modulation of microscopic structure by the confinement, the overall thermal conductivity of the confined fluid can exhibit oscillation with the variation of pore width.

In summary, this work provides a novel way to deepen our understanding about the thermal conductivity of confined fluids. Nevertheless, further improvements of the proposed method are still demanding. On the one hand, more accurate weight function should be designed to reduce the deviation of its theoretical predictions from the simulation results. On the other hand, this work focuses mainly on the atomic LJ fluid, thus it is not applicable to complex fluids, whose molecular has some specific structure. Nonetheless, it is hopeful that this study can shed beneficial light on further investigation on the energy transfer in fluids, especially those of nanoscales.

Acknowledgments

Project supported by the Fundamental Research Fund for the Central Universities of China, and the Research Project for

Independently Cultivate Talents of Hebei Agricultural University (Grant No. ZY2023007).

References

[1] Poling B E, Prausnitz J M and O'Connell J P 2001 *The Properties of Gases and Liquids* (New York: McGrawHill)
[2] Ganvir R B, Walke P V and Kriplani V M 2017 *Renew. Sust. Energ. Rev.* **75** 451
[3] Yuan K J, Shi J M, Aftab W, Qin M L, Usman A, Zhou F, Lv Y, Gao S and Zou R Q 2020 *Adv. Funct. Mater.* **30** 1904228
[4] Galliero G and Boned C 2009 *Phys. Rev. E* **80** 061202
[5] McLinden M O, Klein S A and Perkins R A 2000 *Int. J. Refrig.* **23** 43
[6] Sun T F and Teja A S 2009 *J. Chem. Eng. Data* **54** 2527
[7] Wang X H, Li Y, Yan Y Y, Wright E, Gao N and Chen G M 2020 *Int. J. Refrig.* **119** 316
[8] Arias F J 2023 *Int. J. Heat Mass Transfer* **209** 124111
[9] Zhu J T 2023 *Int. J. Heat Mass Transfer* **209** 124127
[10] Arshad A, Jabbal M and Yan Y Y 2020 *Energ. Convers. Manag.* **205** 112444
[11] Long R, Luo Z Q, Kuang Z F, Liu Z C and Liu W 2020 *Nano Energy* **67** 104284
[12] Wu S F, Yan T, Kuai Z H and Pan W G 2020 *Solar Energy* **205** 474
[13] Zhao Z X, Sun C Z and Zhou R F 2020 *Int. J. Heat Mass Transfer* **152** 119502
[14] Ueki Y, Yamamoto Y, Ohara T and Shibahara M 2023 *Int. J. Heat Mass Transfer* **202** 123746
[15] Giannakopoulos A E, Sofos F, Karakasidis T E and Liakopoulos A 2012 *Int. J. Heat Mass Transfer* **55** 5087
[16] Hyżorek K and Tretiakov K V 2016 *J. Chem. Phys.* **144** 194507
[17] Jin L, Noraldeen S F M, Zhou L P and Du X Z 2022 *Int. J. Heat Mass Transfer* **185** 122325
[18] Chilukoti H K, Kikugawa G, Shibahara M and Ohara T 2015 *Phys. Rev. E* **91** 052404
[19] Zhao Z X, Zhou R F and Sun C Z 2020 *J. Chem. Phys.* **153** 234701
[20] Pozhar L A and Gubbins K E 1993 *J. Chem. Phys.* **99** 8970
[21] Pozhar L A and Gubbins K E 1997 *Phys. Rev. E* **56** 5367
[22] Bugel M and Galliero G 2008 *Chem. Phys.* **352** 249
[23] Lautenschlaeger M P and Hasse H 2019 *Fluid Phase Equilibr.* **482** 38
[24] Sung W and Dahler J S 1984 *J. Chem. Phys.* **80** 3025
[25] Johnson J K, Müller E A and Gubbins K E 1994 *J. Phys. Chem.* **98** 6413
[26] Hoang H and Galliero G 2013 *J. Phys.: Condens. Matter* **25** 485001
[27] Percus J K 1981 *J. Chem. Phys.* **75** 1316
[28] Evans R 1979 *Adv. Phys.* **28** 143
[29] Henderson D 1992 *Fundamentals of Inhomogeneous Fluids* (New York: Dekker)
[30] Yu Y X and Wu J Z 2002 *J. Chem. Phys.* **117** 10156
[31] Roth R, Evans R, Lang A and Kahl G 2002 *J. Phys.: Condens. Matter* **14** 12063
[32] Yu Y X 2009 *J. Chem. Phys.* **131** 024704
[33] Peng B and Yu Y X 2008 *J. Phys. Chem. B* **112** 15407
[34] Yu Y X, Gao G H and Wang X L 2006 *J. Phys. Chem. B* **110** 14418
[35] You F Q, Yu Y X and Gao G H 2005 *J. Phys. Chem. B* **109** 3512
[36] Sun Z L, Kang Y S and Kang Y M 2019 *Chin. Phys. B* **28** 036102
[37] Sun Z L, Kang Y S and Li S T 2022 *J. Phys. Chem. B* **126** 8010
[38] Bitsanis I, Vanderlick T K, Tirrell M and Davis H T 1988 *J. Chem. Phys.* **89** 3152
[39] Rah K and Eu C B 2001 *J. Chem. Phys.* **115** 9370